Physica A 447 (2016) 129–140

Contents lists available at ScienceDirect

Physica A

journal homepage: www.elsevier.com/locate/physa

# Modelling dengue epidemic spreading with human mobility

D.H. Barmak, C.O. Dorso, M. Otero *

*Departamento de Física, Facultad de Ciencias Exactas y Naturales, Universidad de Buenos Aires, Buenos Aires 1428, Argentina*
*IFIBA, CONICET, Ciudad Universitaria, Buenos Aires 1428, Argentina*

## HIGHLIGHTS

- The effect of human mobility on the spatio-temporal dynamics of Dengue is explored.
- Human mobility strongly affects the spread of infection.
- Because of human mobility, multiple foci appear throughout the evolution of the outbreaks.
- The coalescence of these foci with the main one generates a fast spreading of the outbreaks.
- This effect increases the propagation of the outbreak before arrival of the winter season.

## ARTICLE INFO

*Article history:*
Received 8 July 2015
Received in revised form 30 November 2015
Available online 14 December 2015

*Keywords:*
Human mobility
Vector-borne diseases
Foci coalescence
Stochastic modelling

## ABSTRACT

We explored the effect of human mobility on the spatio-temporal dynamics of Dengue with a stochastic model that takes into account the epidemiological dynamics of the infected mosquitoes and humans, with different mobility patterns of the human population. We observed that human mobility strongly affects the spread of infection by increasing the final size and by changing the morphology of the epidemic outbreaks. When the spreading of the disease is driven only by mosquito dispersal (flight), a main central focus expands diffusively. On the contrary, when human mobility is taken into account, multiple foci appear throughout the evolution of the outbreaks. These secondary foci generated throughout the outbreaks could be of little importance according to their mass or size compared with the largest main focus. However, the coalescence of these foci with the main one generates an effect, through which the latter develops a size greater than the one obtained in the case driven only by mosquito dispersal. This increase in growth rate due to human mobility and the coalescence of the foci are particularly relevant in temperate cities such as the city of Buenos Aires, since they give more possibilities to the outbreak to grow before the arrival of the low-temperature season. The findings of this work indicate that human mobility could be the main driving force in the dynamics of vector epidemics.

© 2015 Elsevier B.V. All rights reserved.

## 1. Introduction

Dengue fever is a vector-borne disease caused by a virus of the family *flaviviridae* [1] and transmitted mainly by the mosquitoes *Aedes aegypti* and *Aedes albopictus*.

Newton and Reiter [2] introduced the first SEIR model for dengue in the form of a system of Ordinary Differential Equations (ODE), in which the mosquito population was not modelled. Other ODE models have been developed with

* Corresponding author at: Departamento de Física, Facultad de Ciencias Exactas y Naturales, Universidad de Buenos Aires, Buenos Aires 1428, Argentina.
*E-mail address:* mjotero@df.uba.ar (M. Otero).

http://dx.doi.org/10.1016/j.physa.2015.12.015
0378-4371/© 2015 Elsevier B.V. All rights reserved.

different considerations and assumptions: variability of vector population [3], human population [4], effect of vertical transmission of Dengue in vectors [5], seasonality [6], age structure [7], incomplete gamma distributions for the incubation and infectious times [8] and spatial heterogeneity as well [9].

Focks et al. [10,11] began describing mosquitoes populations by using a Dynamic Table Models, where later the human population and the disease were introduced [12].

Otero and Solari developed a spatially explicit stochastic dengue model [13] which includes the evolution of the mosquitoes population [14,15] but in which humans are considered as a spatially fixed population, i.e. the spatial spreading of the disease is possible only due to mosquito dispersal. Two later models [16,17] modelled the human population as an individual based model and studied the effect of different human mobility patterns on the final size, probability and duration of the epidemic outbreaks.

Recent studies [18–21] suggest that the spatial spreading of a dengue outbreak occurs not only in a diffusive way, but also because of many other secondary foci that appear at spatial scales not compatible with a spatial dynamics driven only by mosquito dispersal. Therefore, it is really important to evaluate the contribution of human mobility to the evolution of the epidemic outbreaks, i.e. the dynamics of the main focus and secondary foci along the dengue outbreaks.

Several works tackle the issue of the correct description of the human beings mobility, relaying on different methods and databases [22–29]. Databases from cellular phone networks, credit cards, hotel reservations, flight reservation databases, etc. are currently used to model human mobility and to study disease spreading. Nevertheless, they could introduce an intrinsic bias on the obtained results because human behaviour can change or adapt in presence of a disease [30–35].

Several studies consider human mobility in human–human transmitted diseases [36,34,37,35,33,38,32,31,39,40], but only a few consider human mobility in vector borne diseases [41–43,17].

In this work we review some details of the model [17] regarding human mobility (Section 2), we present the results of our numerical investigations related to the spatial distribution of recovered individuals, the foci dynamics according to different mobility patterns, the evolution of the main focus of recovered individuals, and an analysis of the contribution of short-range human movements to the evolution of dengue epidemic outbreaks (Section 3). Finally conclusions are drawn in Section 4.

## 2. Theory and calculations

The epidemiological model used in this work has already been published [17]. There are four key processes involved in the dengue contagion and spatial spreading: the epidemiological dynamics of the infected mosquitoes, the epidemiological dynamics of the infected humans, the mobility pattern of the individuals and the mosquito dispersal by flight. From an epidemiological point of view we divided the adult female vector population in three compartments representing the disease status: susceptible (S), exposed (E) and infectious (I), i.e. a *SEI* compartmental model. Humans are considered at the individual level, i.e., with an Individual Based Model (IBM) [16], and follow a susceptible (S), exposed (E), infectious (I) and recovered (R) (SEIR) sequence. In this section we are going to review only some aspects of the model regarding human mobility, for more details about the model and its implementation, we refer to Ref. [17].

The simulation of the evolution of dengue fever is performed in a schematic city (square grid) whose basic unit is the city block (a square of 100 m $\times$ 100 m), in which a human population of 100 individuals is placed. We worked with grids of different sizes: $L = 20$, 50, 100 and 150, being $L$ the side length of the square grid, with $L$ measured in city block units i.e. a grid with $L = 150$ corresponds to a square grid of 150 $\times$ 150 city blocks. The spatial scale simulated goes from small towns ($L = 20$) to a big city ($L = 150$). Mosquito populations were simulated using climatic data tuned to Buenos Aires city, Argentina, and a breeding site density of 400 BS/ha [15,17]. An exposed human (index case) is placed in the centre of the grid, on January 1st, considered as the beginning of the epidemic outbreak $t = 0$.

In order to describe the mobility patterns of the human population we have adopted the same schematic model already presented in Ref. [17]: 50 individuals of each block are randomly selected to be mobile, while the other 50 individuals stay in their original block (Home) during the simulation. Each mobile individual spends 2/3 of the day in its original block (Home), while the other 1/3 of the day the mobile individual stays in a randomly assigned block (Work) according to a particular distribution, which is assigned to each of the mobile individuals. The mobile individuals go to this destination everyday, and at the end of the day they return back to their original block. This random assignment is performed according to certain rules that characterize the human mobility pattern. Following recent works on human mobility (referred in Ref. [17]) the distribution of the displacement lengths of the individuals follow a truncated Levy distribution [23] given by Eq. (1):

$$P(r) \propto (r + r_0)^{-\beta} \exp(-r/\kappa). \tag{1}$$

being $P(r)$ the probability that an individual reaches a distance $r$, where $r_0$, $\beta$ and $\kappa$ are parameters that characterize the distribution.

In this work we have used the parameters shown in Table 1.

The implementation is as follows. One of these distributions is chosen and then each mobile human randomly selects (from this distribution) the distance '$r$ to the "Work" block, with a cut-off equal to $L/2$. This means that the distances are drawn from distributions with a displacement up to half of the city length for all individuals. Once the distance $r$ is chosen the next steps are followed:

**Table 1**
Parameters of the Levy-Flight distribution.

| | $r_0(m)$ | $\beta$ | $\kappa$ (m) |
|---|---|---|---|
| Levy1.65 | 100 | 1.65 | 1500 |
| Levy2 | 100 | 2.00 | 1500 |
| Levy3 | 100 | 3.00 | 1500 |

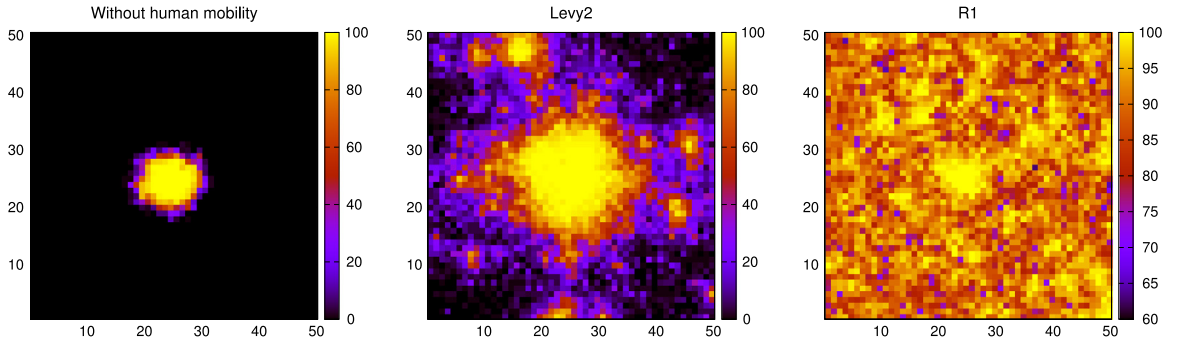


**Fig. 1.** Spatial distribution of recovered individuals for three different conditions: No human mobility (left panel), a human movement pattern according to a Levy-flight distribution with parameter $\beta = 2.00$ (central panel) and a human movement pattern according to a uniform random distribution $R1$ (right panel) for $t = 350$ (after the end of the epidemic outbreak) and a grid size of $50 \times 50$ blocks.

1. $r$ is rounded to its nearest higher integer ($[r] + 1$)
2. Distances from Home block to any other block "$j$" are considered as the nearest integer of the euclidean distances between their centres ($D(j)$)
3. From all blocks whose $D(j) = [r] + 1$, one of them is chosen uniformly.
4. This chosen block will be the work block which the individual will visit everyday

In order to compare these human movement patterns with other reference scenarios, we simulated two other possibilities: the case in which the final destinations of the mobile individuals are assigned according to a uniform random distribution (R1) and the case with no human mobility, in which the spreading of the disease is only due to mosquito dispersal.

## 3. Results and discussion

The main observable in our work is the spatio-temporal distribution of recovered individuals throughout the epidemic outbreaks. In Fig. 1 we analyse the spatial distribution of recovered individuals for three different conditions: No human mobility (left panel), a human movement pattern according to a Levy-flight distribution with parameter $\beta = 2.00$ (central panel) and a human movement pattern according to a uniform random distribution $R1$ (right panel), the three cases for $t = 350$ (at the end of the epidemic outbreak) and a grid size of $50 \times 50$ blocks. Only in the case without human mobility the epidemic outbreaks are restricted to the centre of the grid and display a symmetric shape, while in the other two cases with human mobility (Levy2 and R1) the epidemic outbreaks reach the borders of the grid and present multiple foci. In the case of the Levy-flight distributions the spatial spreading of the epidemic outbreak depends on the value of the $\beta$ parameter, while in the case of the total uniform random distribution $R1$ (showed here as reference for comparison) the epidemic outbreaks always reach the border of the grid for any grid size. In order to understand the mechanisms involved in the spatio-temporal spreading of the disease we are going to study quantitatively the spatial distribution of the recovered individuals and its temporal evolution.

### 3.1. Radial recovered probability function

We define the Radial Recovered Probability Function $g_n(r)$ (Eq. (2)) as a measure of the probability of finding at least "$n$" recovered individuals at a distance "$r$" away from a given reference position, the index case position in the centre of the grid.

$$g_n(r) = \sum_{\substack{\text{Blocks at} \\ \text{a distance } r}} \frac{H\left(\begin{matrix}\#\text{ of recovered} \\ \text{in a block}\end{matrix} - n\right)}{\begin{matrix}\#\text{ Blocks at a} \\ \text{distance } r\end{matrix}} \tag{2}$$

where $H(x)$ is a Heaviside function for discrete variables.

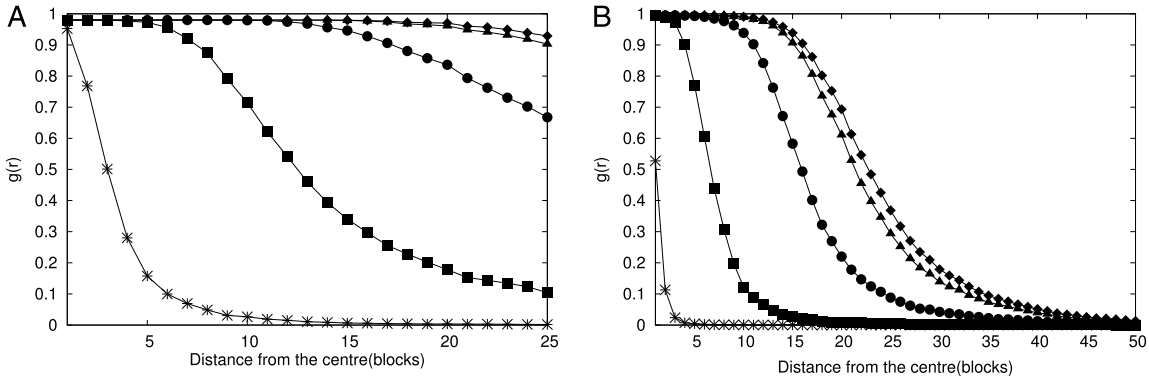


**Fig. 2.** Radial Recovered Probability Function $g_n(r)$, for $\boldsymbol{n} = 10$ and a human movement pattern according to a Levy-flight distribution with parameter $\beta = 1.65$. The left panel (panel A) corresponds to a square grid of size $50 \times 50$ blocks and the right panel (panel B) to a square grid of size $100 \times 100$ blocks. Curves for different times ($t$): star $t = 60$ days, square $t = 90$ days, circle $t = 120$ days, triangle $t = 150$ days and rhombus $t = 190$ days.

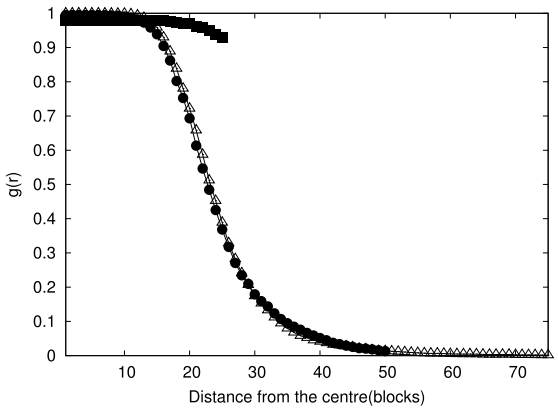


**Fig. 3.** Radial Recovered Probability Function $g_n(r)$, for $\boldsymbol{n} = 10$, a human movement pattern according to a Levy-flight distribution with parameter $\beta = 1.65$ and for $t = 190$. Size of the grid (in blocks): $20 \times 20$ (cross), $50 \times 50$ (square), $100 \times 100$ (circle) and $150 \times 150$ (triangle).

This Radial Recovered Probability Function $g_n(r)$ is calculated for $r \leq \frac{L}{2}$, being $L$ the side length of the square grid, in order to ensure that any angular position can be reached from the centre of the grid, and it is calculated when all the individuals are at home in their original blocks.

Fig. 2 depicts the Radial Recovered Probability Function $g_n(r)$ for $n = 10$ and a human movement pattern according to a Levy-flight distribution with parameter $\beta = 1.65$. The different curves correspond to five different times along the epidemic outbreak: 60, 90, 120, 150 and 190 days after the arrival of the index case. The left panel (panel A) corresponds to a square grid of size $50 \times 50$ blocks and the right panel (panel B) to a square grid of size $100 \times 100$ blocks. In the left panel ($50 \times 50$) we observe that the epidemic outbreak reaches the border of the grid while in the right panel ($100 \times 100$) the borders play an unimportant role in the outbreak, i.e. the probability of finding at least 10 recovered individuals in the border of the grid is lower than 1%.

Fig. 3 shows the Radial Recovered Probability Function $g_n(r)$ for $\boldsymbol{n} = 10$, for a human movement pattern according to a Levy-flight distribution with parameter $\beta = 1.65$ and for a particular day close to the end of the epidemic outbreak (day 190). We observe four curves corresponding to four different grid sizes: $20 \times 20$, $50 \times 50$, $100 \times 100$ and $150 \times 150$ blocks and we perceive that no significant differences can be observed between the curves corresponding to the two largest sizes considered: $100 \times 100$ and $150 \times 150$ blocks (curves with circles and triangles respectively). This result indicates that for the two largest grids studied and consequently for larger ones, the epidemic outbreaks do not reach the border of the grids, being the final size of epidemics independent of the grid size, according to the elimination of any kind of border effects. Nevertheless, for smaller grids the border effects are quite important, meaning that our simulations correspond to cities of different sizes but not for neighbourhoods of different sizes in a city.

### 3.2. Foci dynamics

As it was shown in Fig. 1 the symmetry and compacticity of the spatial density structure of recovered individuals depend on the human mobility pattern. Let us introduce the concept of "focus of recovered individuals" in order to perform an analysis of the spatial structure. Given a city block $i$ we consider that this block is occupied if the number of recovered

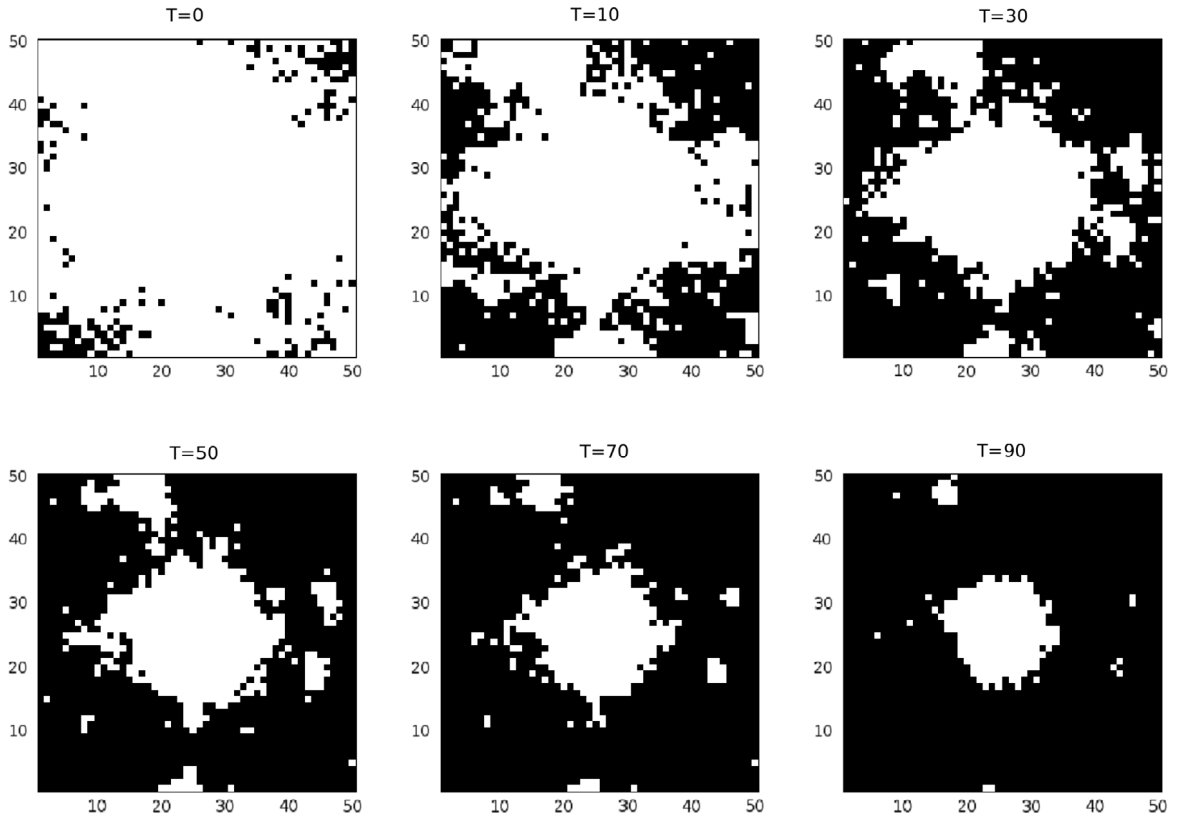


**Fig. 4.** Spatial distribution of occupied blocks according to different thresholds. Simulation conditions: grid of 50 × 50 blocks, human movement pattern according to a Levy-flight distribution with parameter $\beta = 2.00$ and $t = 350$ (end of the epidemic outbreak). A block is white if the number of recovered individuals in that block is higher than a given threshold "$T = 0$, 10, 30, 50, 70 and 90".

individuals in that block is higher than a given threshold $T$. We define a focus as a set of occupied blocks which share at least one neighbour (first and second neighbours) that belongs also to the focus. Then, a block $i$ belongs to a focus $C$ if it satisfies the relation:

$$i \in C \Longleftrightarrow \exists j \in C / i \text{ is neighbour of } j. \tag{3}$$

Fig. 4 illustrates how the choice of the threshold affects the focus structure. The focus splits into smaller pieces as the threshold increases, remaining only those blocks with higher density of recovered individuals.

From Fig. 4 it can be seen that for a threshold of $T = 0$ the epidemic outbreak has reached the whole grid, but for $T = 90$ only the central region is strongly occupied by recovered individuals.

In order to understand the development of the epidemic outbreaks we analyze the temporal evolution of the foci throughout the outbreak. Fig. 5 exhibits the temporal evolution of the number of foci and its dependence on different thresholds for two different grid sizes and human mobility patterns. The top panels (A and B) correspond to a Levy-flight distribution with parameter $\beta = 1.65$ and the bottom panels (C and D) to a Levy-flight distribution with parameter $\beta = 3.0$. Panels A and C correspond to a grid size of 50 × 50 blocks and panels B and D to a grid size of 100 × 100 blocks.

For a human mobility pattern according to a Levy-flight distribution with parameter $\beta = 3.0$ (panels C and D of Fig. 5) we observe that the number of foci grows almost monotonically with time for all the thresholds considered and that the number of foci decreases as the threshold rises. On the contrary, some curves for the Levy-flight distribution with parameter $\beta = 1.65$ show that the number of foci grows, reaches a peak and then goes down until it levels off (for the grid of 50 × 50 blocks, thresholds: $T = 0$ and 10 (panel A) and for the grid of 100 × 100 blocks only for the lowest threshold: $T = 0$ (panel B)). This suggests that two different contrasting effects take place throughout the outbreak. During the outbreak, new foci are being constantly created because of the propagation of the infection. Then these foci begin to merge reducing the final number of foci, but these final remaining foci become larger due to this coalescence process. The different shapes of the curves in Fig. 5 depend on the competition between these two contrasting effects.

In order to study these two effects separately Fig. 6 shows the temporal decrease in the number of foci because of coalescence for different thresholds ($T = 0$, 10 and 30) and for two grid sizes: 50 × 50 blocks (panel A) and 100 × 100 blocks (panel B), and Fig. 7 shows the number of new foci generated day by day (grid sizes: 50 × 50 blocks (panel A)

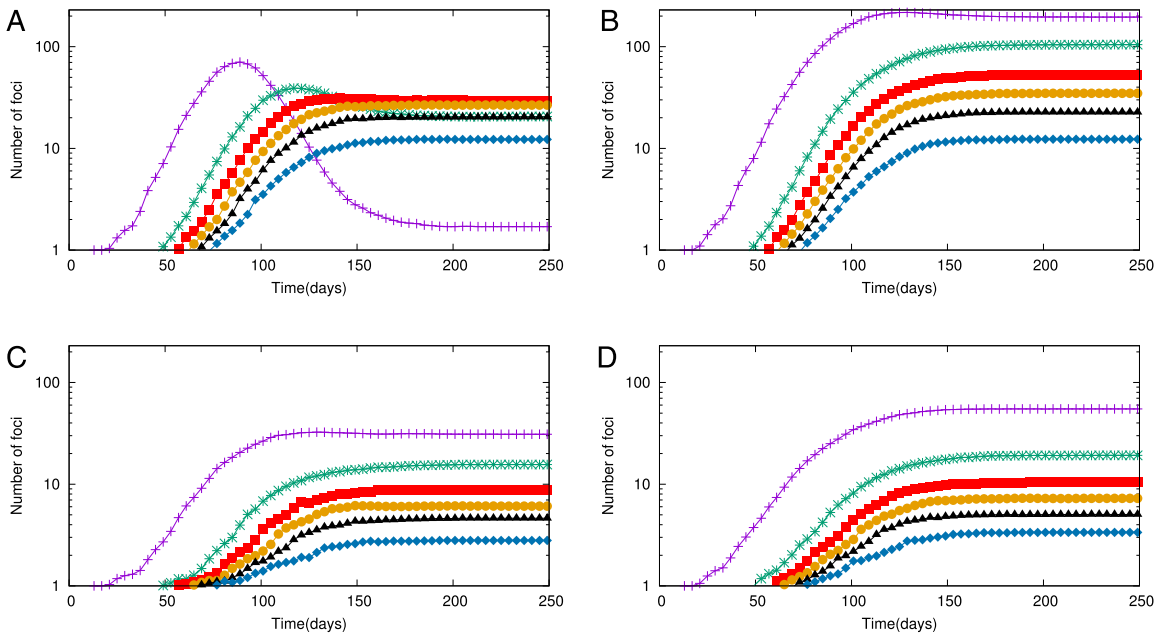


**Fig. 5.** Time evolution of the number of foci for thresholds $T$: cross (violet) 0, star (green) 10, square (red) 30, circle (brown) 50, triangle (black) 70, rhombus (blue) 90. Human mobility pattern and grid sizes (in blocks): panel A: levy1.65—50 × 50, panel B: levy1.65—100 × 100, panel C: levy3—50 × 50 and panel D: levy3—100 × 100. (For interpretation of the references to colour in this figure legend, the reader is referred to the web version of this article.)

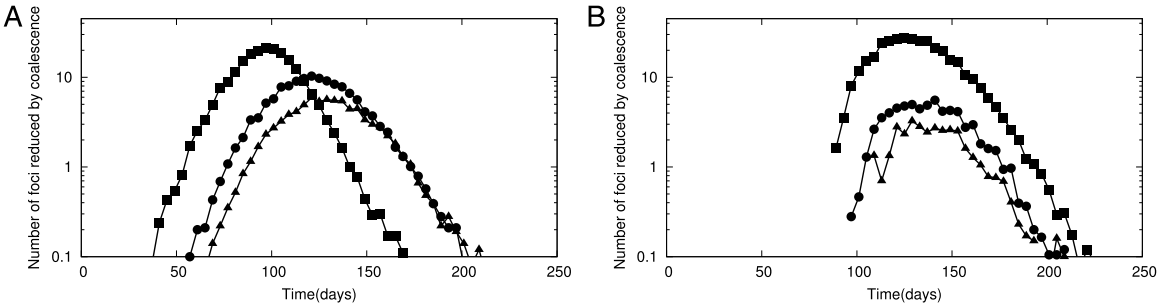


**Fig. 6.** Temporal decrease of the number of foci because of coalescence for thresholds $T$: square 0, circle 10, triangle 30. Panel A: levy1.65—50 × 50, panel B: levy1.65—100 × 100.

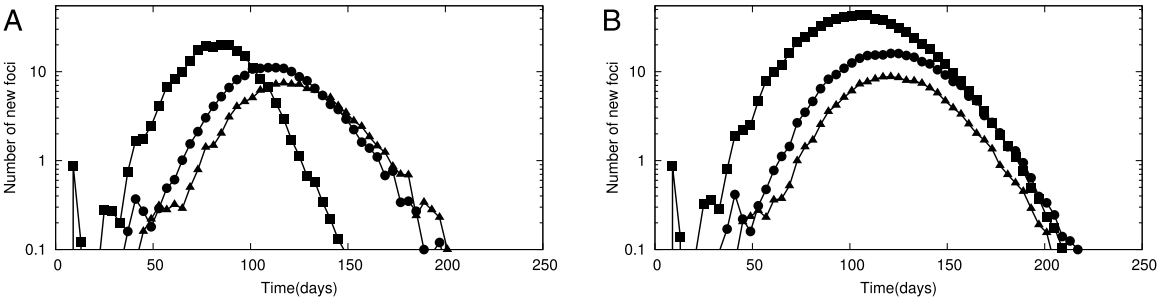


**Fig. 7.** Time evolution of the number of new foci for thresholds $T$: square 0, circle 10, triangle 30. Panel A: levy1.65—50 × 50, panel B: levy1.65—100 × 100.

and 100 × 100 blocks (panel B)), considering as new foci only the ones which do not belong to a pre-existent focus and which appear because the number of recovered individuals in a block reaches a value higher than the threshold considered ($T = 0$, 10 and 30).

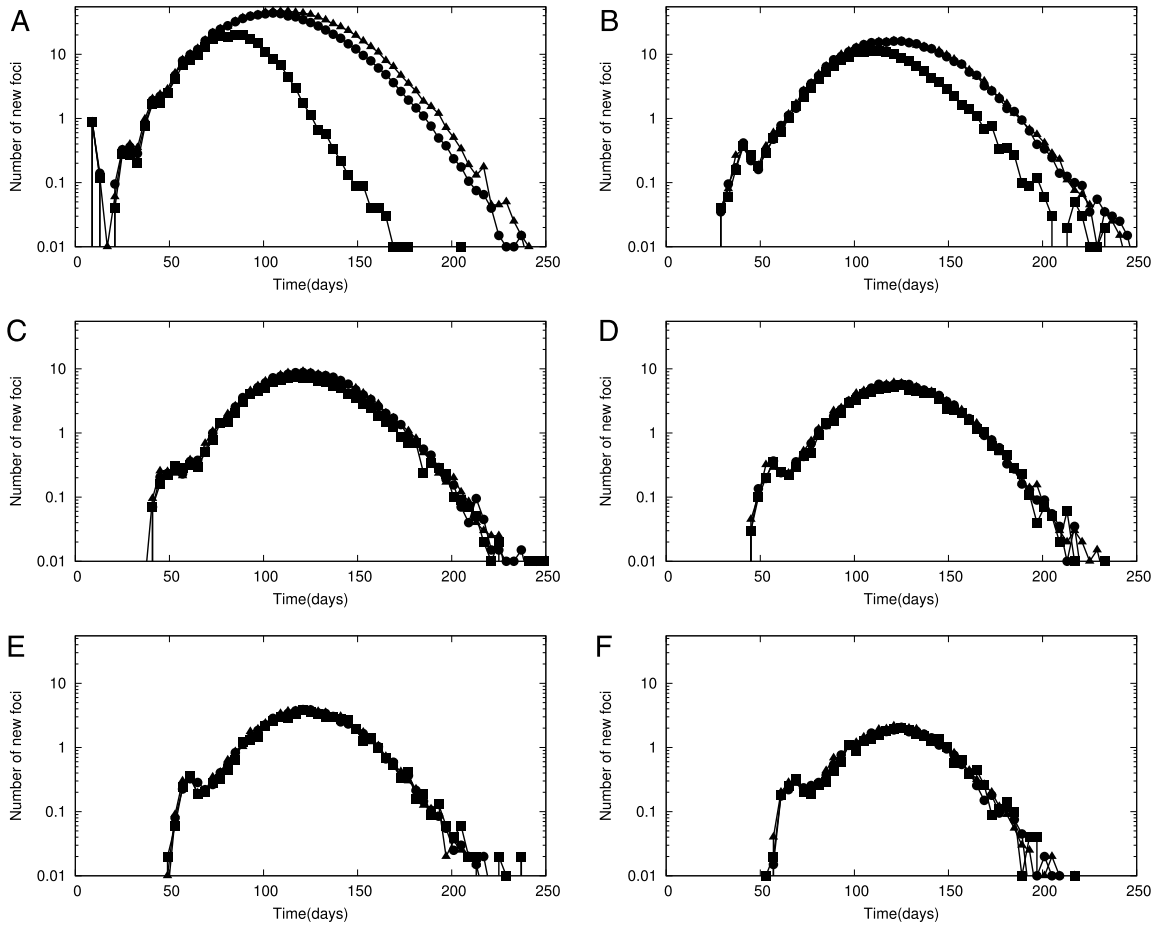


**Fig. 8.** Temporal evolution of the number of new foci for a Levy1.65 distribution and for grid sizes (blocks): square 50 × 50, circle 100 × 100 and triangle 150 × 150. Thresholds $T$: "0 and 10" (panels A and B), "30 and 50" (panels C and D) and "70 and 90" (panels E and F).

For a grid of 50 × 50 blocks we can observe that before day 100 the generation of new foci is greater than the decrease by coalescence, but later this tendency is reverted producing the characteristic maximum observed in Fig. 5. For the grid of 100 × 100 blocks the number of new foci is almost always higher (except for the lowest threshold: $T = 0$) and the peak of the curves are reached approximately 50 days later than the case of the grid of 50 × 50.

Fig. 7 reveals an apparent shift of the peak of new foci for the grid of size 50 × 50 blocks and the lowest threshold ($T = 0$) respect to higher thresholds, i.e. the peak of the number of new foci is reached later for higher thresholds in the same grid. In order to study these observations we compared the temporal evolution of the number of new foci (Fig. 8) for three grid sizes (50 × 50, 100 × 100 and 150 × 150 blocks), for the Levy-flight distribution with parameter $\beta = 1.65$ and for six different thresholds $T$: "0 and 10" (panels A and B), "30 and 50" (panels C and D) and "70 and 90" (panels E and F). At the beginning of the outbreak the curves for threshold $T = 0$ are similar up to a particular moment in which the number of new foci stops growing and begins to decrease. The difference in the temporal evolution of the new foci becomes smaller as the threshold increases, in fact there are differences in the number of new foci between grids of sizes 100 × 100 blocks and 150 × 150 blocks only for the lowest threshold considered ($T = 0$). A situation which supports the idea of the disappearance of border effects for larger grid sizes (Fig. 3).

Fig. 9 depicts the normalized difference of the final size of epidemics ($ND$) for the grids of sizes 50 × 50 blocks and 100 × 100 blocks. We observe that the difference between the two cases studied is lower than 10% throughout the whole outbreak.

As the final size of epidemics is similar for the grids of 50 × 50, 100 × 100 and 150 × 150 blocks, the density of recovered individuals must be greater for the smaller grids. Since at time $t = 0$ there is only one infected individual, the larger the system, the lower the initial density. Therefore, it takes longer to reach the same density of infected individuals (see Eq. (2) in Ref. [44]), which is not possible because winter begins at time $t \approx 190$. As a consequence, when $L$ increases, the final density of recovered individuals decreases.

This means that there are less unoccupied blocks in the smaller grids, considering an occupied block as a block with a number of recovered individuals higher than the threshold. This situation is more important for low thresholds and small

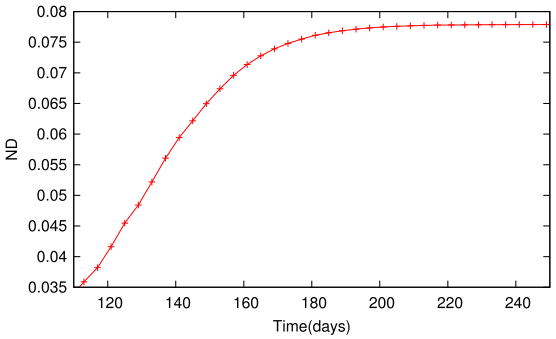


**Fig. 9.** Normalized difference (*ND*) of the final size of epidemics between a grid of size 100 × 100 blocks and a grid of size 50 × 50 blocks, for a Levy-flight distribution Levy1.65.

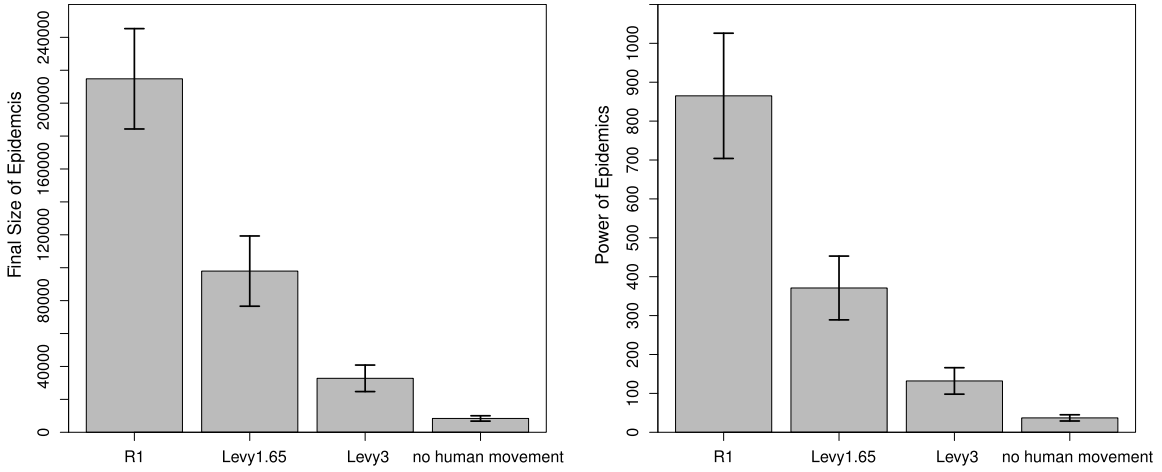


**Fig. 10.** Final Size of Epidemics and Power of the Epidemics for a grid of 50 × 50 blocks, 400 BS/ha and human movements: R1, Levy1.65, Levy3 and the case without human movement as reference.

grid sizes. If there is less space for the same amount of occupied blocks then there will be less space for the emergence of new foci and the probability that two or more foci merge will be higher, as shown in Figs. 5 and 6.

### 3.3. The largest focus

In order to continue the analysis of the spatial spreading of the disease we study how the size and mass of the foci are spatially distributed. We define the "size of the focus" $S_f$ as the number of blocks belonging to a focus and the "mass of the focus" $M_f$ as the number of recovered individuals present in a focus.

We define two other new measures (respect to a threshold $T$ of recovered humans): the size proportion of the largest focus ($S_p(T)$) and the mass proportion of the largest focus ($M_p(T)$). $S_p(T)$ and $M_p(T)$ are defined by Eqs. (4) and (5) respectively.

$$S_p(T) = \frac{\text{Number of blocks with at least } T \text{ recovered humans in the largest focus}}{\text{Number of blocks with at least } T \text{ recovered humans}} \tag{4}$$

$$M_p(T) = \frac{\text{Number of recovered humans in blocks with at least } T \text{ recovered humans in the largest focus}}{\text{Number of recovered humans in blocks with at least } T \text{ recovered humans}} \tag{5}$$

where the largest focus is the one with the highest population of recovered individuals.

For the analysis of the spatial spreading of the disease we performed simulations in a grid of 50 × 50 for three different distributions of human movement: Levy1.65, Levy3 and R1. For these simulations the Final Size of Epidemics (record of the total recovered individuals along the outbreak) and the Power of the Epidemics (ratio between the median of the final size of the epidemics and the median of the duration of the epidemics) [17] are shown in Fig. 10. We can observe that the distributions characterized by longer jumps produce larger epidemic outbreaks (Left panel of Fig. 10). Since the end of the epidemic outbreaks is because of the arrival of the winter season [17], the Power of the Epidemics is meanly determined exclusively by the Final Size of Epidemics (Left panel of Fig. 10).

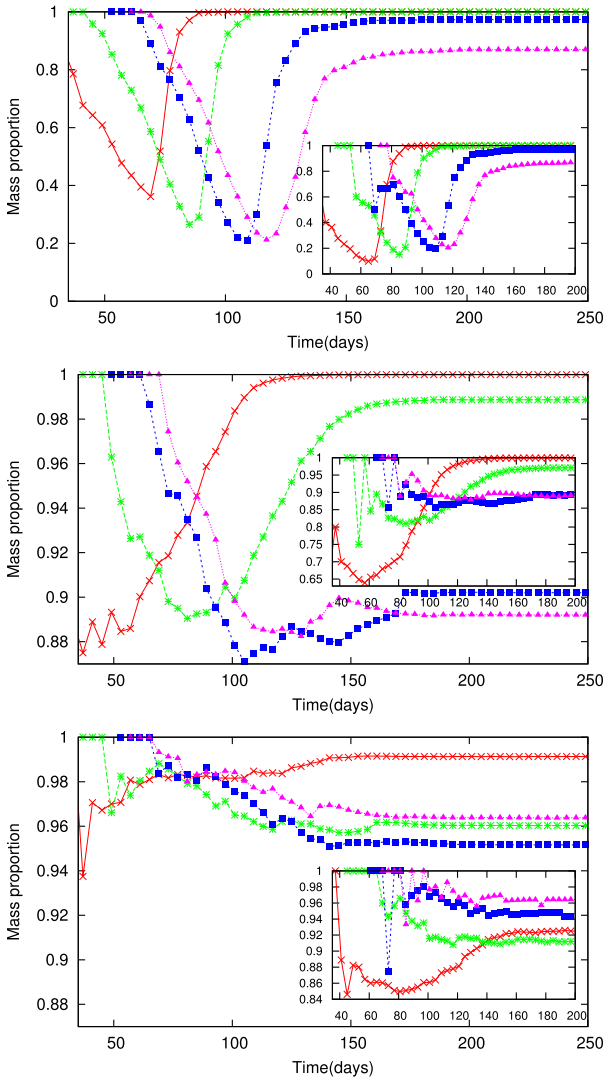


**Fig. 11.** $M_p(T)$ and $S_p(T)$ (inset) for a grid of size of 50 × 50 blocks, thresholds $T$: cross (red) 0, star (green) 10, square (blue) 70 and triangle (violet) 90. Human movement patterns: R1 (top), Levy1.65 (middle) and Levy3 (bottom). (For interpretation of the references to colour in this figure legend, the reader is referred to the web version of this article.)

Fig. 11 shows the temporal evolution of $M_p(T)$ and $S_p(T)$ (insets) for different thresholds ($T = 0, 10, 70$ and 90) and for three different human movement patterns studied: uniform random R1 (top panel) and Levy-flight distributions with parameters $\beta = 1.65$ (central panel) and $\beta = 3.00$ (bottom panel).

For both of the Levy-flight distributions studied, more than 85% of the mass is concentrated in the largest focus. Although the total number of foci can reach approximately one hundred foci (see Fig. 5), one single focus concentrates the largest number of recovered individuals. For the particular case of the Levy-flight distribution with parameter $\beta = 1.65$ we observe a fast growth of the mass ratio for the lower thresholds ($T = 0$ and 10), which is not observed for the other thresholds studied. The largest focus is growing faster because of the coalescence of smaller foci with high density of recovered individuals.

The temporal evolution of the size ratio is qualitatively similar but the values reached are lower compared to the mass ratio values. This happens because most of the foci that do not belong to largest focus have low density of recovered individuals, affecting mostly the size ratio than the mass ratio.

For the R1 distribution both ratios reach values as low as 20%. This is consistent with this human movement pattern in which the main focus does not play a central role in the spreading of the disease because of the high number of secondary foci that appears in the early stages of the outbreak. Nevertheless, all these foci tend to merge throughout the outbreak. On the contrary, the results obtained for the Levy-flight patterns suggest that the growth of the epidemic outbreak occurs mostly from a main central focus such as in the case without human mobility, but with a higher speed.

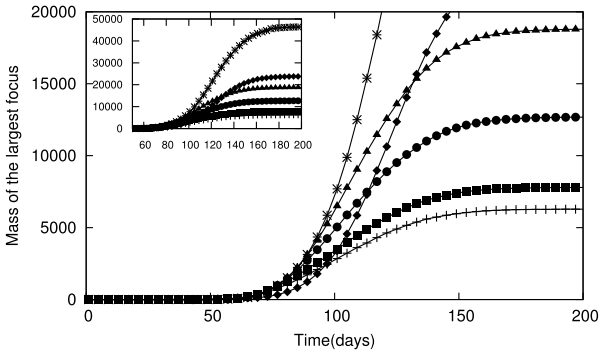


**Fig. 12.** Mass of the largest focus for a grid of $50 \times 50$ blocks, a threshold $T = 70$ and for different human movement patterns: without human movement (cross), Levy1.65 (star), Levy1.65 with a cut-off value at $D = 1$ (square), Levy1.65 with a cut-off value at $D = 3$ (circle), Levy1.65 with a cut-off value at $D = 5$ (triangle), Levy1.65 without mosquito dispersal (rhombus). Inset: same results in an expanded $y$-axis scale.

### 3.4. Difussion vs. jumps

In order to study the evolution of this central focus throughout the outbreak, Fig. 12 displays the temporal evolution of the mass of the largest focus ($M_f$ of the largest focus) for a grid size of $50 \times 50$ blocks, a threshold of $T = 70$ and for different scenarios. The curve with cross symbols corresponds to the case without human movement and the one with star symbols to a Levy-flight distribution with $\beta = 1.65$. We can observe that the mass of the largest focus without human mobility is almost five times smaller than in the case of the Levy-flight distribution (see inset of Fig. 12).

Since we want to evaluate the contribution of the short-range movements of this distribution to the disease spreading, we performed simulations with a Levy-flight distribution for different cut-off distances $D$ with $D = 1$, 3 and 5 blocks (Curves with squares, circles and triangles of Fig. 12 respectively). For example, in a Levy-flight distribution with a cut-off of $D = 5$ (curve with circles), every jump to a distance greater than five blocks does not occur, remaining the individuals involved in their original blocks. The aim of these simulations is the study of the temporal evolution of the size of the largest focus and its growth speed, only due to the short-range human movements, and then compare them with the situation without human movement. We refer as "short-range human movements", those movements that contribute to the spreading of the disease so that the outbreak grows as one single central focus just as in the diffusive case without human movement. The results of these simulations are shown in Fig. 12 (curves with squares ($D = 1$), circles ($D = 3$) and triangles ($D = 5$)) and reveal that the final mass and the growth speed of the largest focus decrease as the cut-off distances decrease.

On the other hand we performed simulations with human mobility according to a Levy-flight distribution with $\beta = 1.65$, in which mosquito dispersal was cancelled in order to study the spreading of the disease purely due to human movement (curve with rhombus of Fig. 12). The results of these simulations point out that the epidemic outbreaks spread even without mosquito dispersal, reaching final sizes of epidemics %50 lower than in the case with vector dispersal. In the early stages of the epidemic outbreak the mass growth of the largest focus is slower than in the cases with flights but then the growth speed increases so that the final size reaches a value higher than those obtained for the Levy-flights with different cut-offs. We notice also that the effects of human mobility and vector dispersal are not independent since the temporal evolution for the levy flight distribution with vector dispersal cannot be constructed by addition of the results obtained for the cases in which the spreading were mediated purely by human movement and mosquito dispersal.

We observed previously in Fig. 5 that for every threshold studied the number of foci for the Levy1.65 movement was higher than for the Levy3 movement, but we showed no information about the mass and size distributions of the foci. Fig. 13 depicts the size and mass distributions of the foci for the day $t = 90$, a grid of size $50 \times 50$ blocks, four different thresholds $T = 0$, 10, 70 and 90 and two human movements: Levy 1.65 and Levy3. We selected a moment of the outbreak $t = 90$ in which the decrease of the foci by coalescence begins to be more important than the generation of new foci (for the Levy1.65 movement). It can be seen that the distributions of masses (panels B and D) and sizes (panels A and C) appear to follow a power law for low values. Beyond this behaviour, we observed a peak corresponding to the largest focus. It is interesting to notice here that for all sizes and masses, the number of foci is greater in the case of a Levy1.65 movement than in the case of a levy3 movement.

## 4. Conclusions

In this work we have explored the effect of human mobility on the spatio-temporal dynamics of Dengue with an epidemiological model developed in our group [17]. Four main processes involved in the dengue contagion and spatial spreading are considered in our model: the epidemiological dynamics of the infected mosquitoes, the epidemiological dynamics of the infected humans, different mobility patterns of the human population and the mosquito dispersal.

From our results we can conclude that human mobility strongly increases the spread of infection, not only by increasing the final size of epidemics but also by changing the morphology of the epidemic outbreak. When the spreading of the

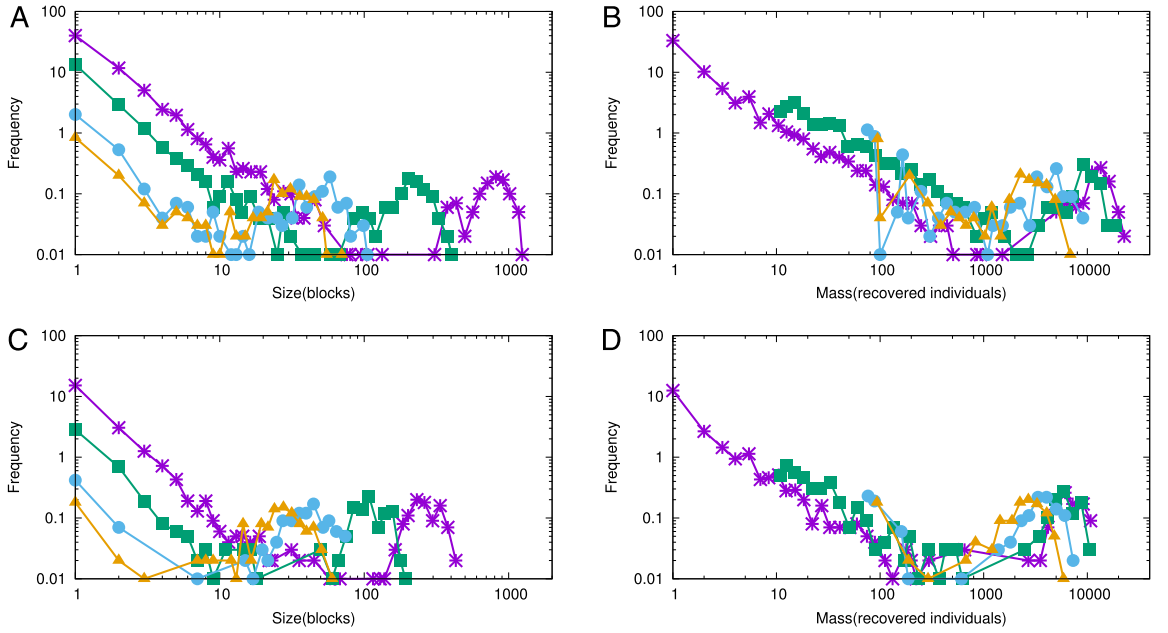


**Fig. 13.** Focus distribution for $t = 90$ according to focus size (panels A and C) and focus mass (panels B and D), for a grid of size $50 \times 50$ blocks, and thresholds $T$: 0 (violet star), 10 (green square), 70 (light blue circle), 90 (brown triangle). Human movement patterns: Levy1.65 (panels A and B) and Levy3 (panels C and D). (For interpretation of the references to colour in this figure legend, the reader is referred to the web version of this article.)

disease is driven only by the mosquitoes, a single focus occurs which expands due to the diffusive dynamics associated with their dispersal. Instead, when human mobility is considered, multiple foci appear in the course of evolution. Human mobility increases the final size of the epidemic, the speed of propagation and the morphology of the epidemic outbreaks. Nevertheless, since the end of the outbreaks is governed by the arrival of the winter, the duration of the epidemic outbreaks is not sensitive to the different human mobility patterns. Therefore, the power of the epidemics is determined exclusively by the final size of the epidemics.

The secondary foci could be of little importance according to their mass or size compared with the largest main focus. However, the union of these foci with the main one generates an effect, through which the latter attains a size greater than the one obtained in the case without human mobility, e.g.: for a Levy flight 1.65 the mass of the largest focus is ten times higher than the mass of the focus obtained in the case of epidemic outbreaks spread only with mosquito dispersal. The increase in growth rate due to human mobility and the coalescence of the foci is particularly relevant in temperate cities such as the city of Buenos Aires, since it gives more possibilities to the outbreak to grow before the arrival of the winter.

The findings of this work indicate that human mobility could be the *main* driving force in the dynamics of vector epidemics. Human movement results in a faster and extended epidemic dynamics. Given this situation, when measures are thought to combat or attenuate the spread of epidemics, human mobility must be one of the major points to be considered.

## Acknowledgement

We acknowledge the support of the University of Buenos Aires (Argentina) through grant UBACyT 20020110100205.

## References

[1] D.J. Gubler, Dengue and dengue hemorrhagic fever, Clin. Microbiol. Rev. 11 (1998) 480–496.
[2] E.A.C. Newton, P. Reiter, A model of the transmission of dengue fever with an evaluation of the impact of ultra-low volume (ULV) insecticide applications on dengue epidemics, Am. J. Trop. Med. Hyg. 47 (1992) 709–720.
[3] L. Esteva, C. Vargas, Analysis of a dengue disease transmission model, Math. Biosci. 150 (1998) 131–151.
[4] L. Esteva, C. Vargas, A model for dengue disease with variable human population, J. Math. Biol. 38 (1999) 220–240.
[5] L. Esteva, C. Vargas, Influence of vertical and mechanical transmission on the dynamics of dengue disease, Math. Biosci. 167 (2000) 51–64.
[6] L.M. Bartley, C.A. Donnelly, G.P. Garnett, The seasonal pattern of dengue in endemic areas: Mathematical models of mechanisms, Trans. R. Soc. Trop. Med. Hyg. 96 (2002) 387–397.
[7] P. Pongsumpun, I.M. Tang, Transmission of dengue hemorrhagic fever in an age structured population, Math. Comput. Modelling 37 (2003) 949–961.
[8] G. Chowell, P. Diaz-Dueñas, J. Miller, A. Alcazar-Velazco, J. Hyman, P. Fenimore, C. Castillo-Chavez, Estimation of the reproduction number of dengue fever from spatial epidemic, Math. Biosci. 208 (2007) 571–589.
[9] C. Favier, D. Schmit, C.D.M. Müller-Graf, B. Cazelles, N. Degallier, B. Mondet, M.A. Dubois, Influence of spatial heterogeneity on an emerging infectious disease: The case of dengue epidemics, Proc. R. Soc. Lond. Biol. Sci. 272 (1568) (2005) 1171–1177.
[10] D.A. Focks, D.C. Haile, E. Daniels, G.A. Moun, Dynamics life table model for *Aedes aegypti*: Analysis of the literature and model development, J. Med. Entomol. 30 (1993) 1003–1018.

[11] D.A. Focks, D.C. Haile, E. Daniels, G.A. Mount, Dynamic life table model for *Aedes aegypti*: Simulations results, J. Med. Entomol. 30 (1993) 1019–1029.
[12] D.A. Focks, D.C. Haile, E. Daniels, D. Keesling, A simulation model of the epidemiology of urban dengue fever: literature analysis, model development, preliminary validation and samples of simulation results, Am. J. Trop. Med. Hyg. 53 (1995) 489–505.
[13] M. Otero, H.G. Solari, Mathematical model of dengue disease transmission by *Aedes aegypti* mosquito, Math. Biosci. 223 (2010) 32–46.
[14] M. Otero, H.G. Solari, N. Schweigmann, A stochastic population dynamic model for *Aedes Aegypti*: Formulation and application to a city with temperate climate, Bull. Math. Biol. 68 (2006) 1945–1974.
[15] M. Otero, N. Schweigmann, H.G. Solari, A stochastic spatial dynamical model for Aedes aegypti, Bull. Math. Biol. 70 (2008) 1297–1325.
[16] M. Otero, D.H. Barmak, C.O. Dorso, H.G. Solari, M.A. Natiello, Modeling dengue outbreaks, Math. Biosci. 232 (2) (2011) 87–95.
[17] D.H. Barmak, C.O. Dorso, M. Otero, H.G. Solari, Dengue epidemics and human mobility, Phys. Rev. E E84 (2011) 011901.
[18] K.A. Liebman, S.T. Stoddard, A.C. Morrison, C. Rocha, S. Minnick, M. Sihuincha, K.L. Russell, J.G. Olson, P.J. Blair, D.M. Watts, T. Kochel, T.W. Scott, Spatial dimensions of dengue virus transmission across interepidemic and epidemic periods in iquitos, peru (1999–2003), PLoS Negl. Trop. Dis. 6 (2) (2012) e1472. http://dx.doi.org/10.1371/journal.pntd.0001472.
[19] G.M. Vazquez-Prokopec, U. Kitron, B. Montgomery, P. Horne, S.A. Ritchie, Quantifying the spatial dimension of dengue virus epidemic spread within a tropical urban environment, PLoS Negl. Trop. Dis. 4 (12) (2010) e920. http://dx.doi.org/10.1371/journal.pntd.0000920.
[20] A.C. Morrison, A. Getis, M. Santiago, J. Rigau-Perez, P. Reiter, Exploratory space–time analysis of reported dengue cases during an outbreak in florida, puerto rico, 1991–1992, Am. J. Trop. Med. Hyg. 58 (3) (1998) 287–298.
[21] C. Rotela, F. Fouque, M. Lamfri, P. Sabatier, V. Introini, M. Zaidenberg, C. Scavuzzo, Space–time analysis of the dengue spreading dynamics in the 2004 Tartagal outbreak, northern Argentina, Acta Trop. 103 (2007) 1–13.
[22] I. Rhee, M. Shin, S. Hong, K. Lee, S. Chong, On the levy-walk nature of human mobility: do humans walk like monkeys?, Tech. Rep., Computer Science Department, North Carolina State University, 2007.
[23] M.C. Gonzalez, C.A. Hidalgo, A.-L. Barabasi, Understanding individual human mobility patterns, Nature 453 (2008) 779–782.
[24] D. Brockmann, L. Hufnagel, T. Geisel, The scaling laws of human travel, Nature 439 (2006) 462–465.
[25] L.H.D. Brockmann, The Scaling Law of Human Travel—A Message from George, World Scientific, 2007.
[26] G. Chowell, J.M. Hyman, S. Eubank, C. Castillo-Chavez, Scaling laws for the movement of people between locations in a large city, Phys. Rev. E 68 (6) (2003) 661021–661027.
[27] C. Cattuto, W. Van den Broeck, A. Barrat, V. Colizza, J.-F. Pinton, A. Vespignani, Dynamics of person-to-person interactions from distributed rfid sensor networks, PLoS One 5 (2010) e11596. http://dx.doi.org/10.1371%2Fjournal.pone.0011596.
[28] J. Candia, M.C. Gonzalez, P. Wang, T. Schoenharl, G. Madey, A. laszlo Barabasi, Uncovering individual and collective human dynamics from mobile phone records, J. Phys. A 41 (22) (2008) http://dx.doi.org/10.1088/1751-8113/41/22/224015.
[29] P. Wang, M.C. Gonzalez, Understanding spatial connectivity of individuals with non-uniform population density, Philos. Trans. R. Soc. Lond. Ser. A 367 (2009) 3321–3329. http://dx.doi.org/10.1098/rsta.2009.0089.
[30] J.M. Epstein, J. Parker, D. Cummings, R.A. Hammond, Coupled contagion dynamics of fear and disease: Mathematical and computational explorations, PLoS One 3 (2008) e3955. http://dx.doi.org/10.1371%2Fjournal.pone.0003955.
[31] D.H. Zanette, S.R. Gusman, Infection spreading in a population with evolving contacts, J. Biol. Phys. 34 (2007) 135–148.
[32] W. Lig, Y. Jia-Ren, Z. Jian-Guo, L. Zi-Ran, Controlling disease spread on networks with feedback mechanism, Chin. Phys. 16 (9) (2007) 2498+. http://dx.doi.org/10.1088/1009-1963/16/9/002.
[33] N.H. Fefferman, K.L. Ng, How disease models in static networks can fail to approximate disease in dynamic networks, Phys. Rev. E 76 (3) (2007) 031919+. http://dx.doi.org/10.1103/PhysRevE.76.031919.
[34] S. Funk, M. Salathé, V.A.A. Jansen, Modelling the influence of human behaviour on the spread of infectious diseases: a review, J. R. Soc. Interface 7 (50) (2010) 1247–1256. http://dx.doi.org/10.1098/rsif.2010.0142.
[35] Z. Zhao, J.P. Calderón, C. Xu, G. Zao, D. Fenn, D. Sornette, R. Crane, P.M. Hui, N.F. Johnson, Effect of social group dynamics on contagion, Phys. Rev. E 81 (5) (2010) 056107+. http://dx.doi.org/10.1103/PhysRevE.81.056107.
[36] A. Buscarino, L. Fortuna, M. Frasca, V. Latora, Disease spreading in populations of moving agents, Eur. Phys. Lett. 82 (3) (2008) 38002.
[37] X. Li, L. Cao, G.F. Cao, Epidemic prevalence on random mobile dynamical networks: individual heterogeneity and correlation, Eur. Phys. J. B 75 (2010) 319–326. http://dx.doi.org/10.1140/epjb/e2010-00090-9.
[38] M. Keeling, K.T. Eames, Networks and epidemic models, J. R. Soc. Interface 2 (4) (2005) 295–307. http://dx.doi.org/10.1098/rsif.2005.0051.
[39] S. Risau-Gusmans, D.H. Zanette, Contact switching as a control strategy for epidemic outbreaks, J. Theoret. Biol. 257 (1) (2009) 52–60. http://dx.doi.org/10.1016/j.jtbi.2008.10.027.
[40] T. Gross, C.J. D'Lima, B. Blasius, Epidemic dynamics on an adaptive network, Phys. Rev. Lett. 96 (20) (2006) 208701+. http://dx.doi.org/10.1103/PhysRevLett.96.208701.
[41] P. Pongsumpun, D.G. Lopez, C. Favier, L. Torres, J. Llosa, M. Dubois, Dynamics of dengue epidemics in urban contexts, Trop. Med. Int. Health 13 (2008) 1180–1187.
[42] S.T. Stoddard, A.C. Morrison, G.M. Vazquez-Prokopec, V.P. Soldan, T.J. Kochel, U. Kitron, J.P. Elder, T.W. Scott, The role of human movement in the transmission of vector-borne pathogens, PLoS Negl. Trop. Dis. 3 (7) (2009) e481. http://dx.doi.org/10.1371/journal.pntd.0000481.
[43] L. Sattenspiel, The Geographic Spread of Infectious Diseases: Models and Applications, Princeton University, 2009.
[44] M. Barthélemy, A. Barrat, R. Pastor-Satorras, A. Vespignani, Dynamical patterns of epidemic outbreaks in complex heterogeneous networks, J. Theoret. Biol. 235 (2005) 275–288.